Article

Study on Flow Characteristics of Flue Gas and Steam Co-Injection for Heavy Oil Recovery

Yanmin Ji [1], Boliang Li [2], Zongyuan Han [1], Jian Wang [1], Zhaomin Li [2] and Binfei Li [2,*]

1   Lusheng Petroleum Development Company Limited, SINOPEC Shengli Oilfield Company, Dongying 257000, China
2   School of Petroleum Engineering, China University of Petroleum (East China), Qingdao 266580, China
*   Correspondence: libinfei999@126.com

Abstract: Flue gas is composed of N_2 and CO_2, and is often used as an auxiliary agent for oil displacement, with good results and very promising development prospects for co-injection with steam to develop heavy oil. Although research on the oil displacement mechanism of flue gas has been carried out for many years, the flow characteristics of steam under the action of flue gas have rarely been discussed. In this paper, the flow resistance and heat transfer effect of flue gas/flue gas + steam were evaluated by using a one-dimensional sandpack, a flue gas-assisted steam flooding experiment was carried out using a specially customized microscopic visualization model, and the microscopic flow characteristics in the process of the co-injection of flue gas and steam were observed and analyzed. The results showed that flue gas could improve the heat transfer effect of steam whilst accelerating the flow of steam in porous media and reducing the flow resistance of steam. Compared with pure steam, when the volume ratio of flue gas and steam was 1:2, the mobility decreased by 2.8 and the outlet temperature of the sandpack increased by 35 °C. This trend intensified with an increase in the proportion of flue gas. In the microscopic oil displacement experiments, the oil recovery and sweep efficiency of the flue gas and steam co-injection stage increased by 4.7% and 32.9%, respectively, compared with the pure steam injection stage due to the effective utilization of blocky remaining oil and corner remaining oil caused by the expansion of fluid channels, the flow of flue gas foam, and the dissolution and release of flue gas in heavy oil.

Keywords: flue gas; steam; heavy oil; flow characteristic; microscopic experiment

1. Introduction

Heavy oil refers to crude oil with a viscosity greater than 50 mPa·s under reservoir conditions or with a viscosity greater than 100 mPa·s after degassing [1]. It is characterized by a low wax content, a low freezing point, high contents of colloid and asphaltene, and a high viscosity, and is an important raw material for processing high-grade asphalt, high-end motor oil, aerospace fuels, etc. [2,3]. Worldwide, heavy oil resources are abundant. According to statistics, the total resources of bitumen and heavy oil in the world are about 9380×10^8 t, mainly distributed in Canada, Venezuela, and the United States [4,5]. Today, with the gradual reduction in light crude oil reserves, how to continuously and efficiently develop and utilize these heavy oil resources is a major challenge to meet the rapidly growing energy consumption demand and ensure stable social operation [6,7].

The poor mobility of heavy oil under reservoir condition makes the working of conventional oil displacement techniques difficult. Thermal recovery is currently a widely used method, mainly including cyclic steam stimulation (CSS), steam-assisted gravity drainage (SAGD), steam flooding, and in situ combustion [8–10]. Based on the current status of oil and gas development in China, CSS and SAGD technologies dominate the development of heavy oil, but the technology itself has several limitations such as large heat loss in the wellbore, steam gravity override, viscous fingering of steam, and channeling

in heterogeneous reservoirs, which lead to a significant reduction in steam dryness and heat sweep efficiency [11–13]. The resulting negative effects are further exacerbated as the development cycle increases [14]. Therefore, it is necessary to propose new methods for the efficient development of heavy oil.

In today's low-carbon society, flue gas-assisted steam development for heavy oil is again in the spotlight [15–18]. The feasibility of flue gas and steam co-injection technology has been verified in several field trials over the last century [19,20] and this method is more economical than others that enhance heavy oil recovery, especially using today's more mature flue gas re-injection equipment. Compared with other gases (N_2 and CO_2), flue gas comes from steam boilers, eliminating the cost of compression and transportation, and the cost of gas is extremely low. Compared with solvents and chemical methods to improve heavy oil recovery, there is no need to develop expensive displacement media that can adapt to reservoir conditions and it will not cause secondary damage to the reservoir. In addition, the removal of dust, sulfur, and oxygen from the flue gas prior to injection into the formation is a prerequisite for the use of this technology in the field to ensure safety and environmental protection. In summary, flue gas and steam co-injection technology not only enhances the recovery of thick oil, but also mitigates global warming by utilizing greenhouse gases as a resource. Relevant research shows that when flue gas and steam flow together under the influence of the physical properties of non-condensable gas, the heat dissipation coefficient of steam is reduced and the heat utilization and oil displacement efficiency of the oil displacement process is improved [21,22]. At the same time, nitrogen and carbon dioxide affect the physical properties of heavy oil (viscosity, volume coefficient, interfacial tension, etc.) [23–27], recover the light components of heavy oil through extraction [28], effectively supplement the formation pressure, increase the oil production rate, and advance the oil production time [29]. Although CO_2 can lead to the aggregation and deposition of asphaltenes and the blocking of rock pores [28], this negative effect is far less than the benefit it brings.

In general, the development of heavy oil by steam is a process of coupling of heat, fluid, and solid fields. Changes in the steam temperature, fluid composition, and reservoir type have a great impact on the flow characteristics of the fluid. For example, during experiments and simulations, the bottom-hole dryness of injected steam has been raised as much as possible to optimize the oil displacement effect [30,31]. Although the heat carried by steam increased, the flow resistance in the formation also increased and the dryness of steam along the way decreased faster, and the heat loss along the way increased [32], which does not improve economic efficiency when applied in the field. With the addition of flue gas, the fluid flow process becomes more complex when steam develops heavy oil and non-condensable gas is added to the gas phase in addition to steam. For a multiphase flow, the displacement pressure of a two-phase flow is generally greater than that of a single-phase flow, and the resistance of a three-phase flow is greater than that of a two-phase flow [33–36]. However, the influence of the gas phase composition on an oil, gas, and water three-phase composite flow has not been clarified in current relevant studies. In addition to the phase state, flue gas also has a great impact on the dryness of steam, which has attracted the attention of many scholars in recent years [37,38]. Although studies on flue gas-assisted steam development for heavy oil have been conducted for many years, most of the attention has been focused on the oil enhancement mechanism of flue gas to improve recovery, and few discussions have been conducted on the characteristics of steam seepage under the action of flue gas. In addition, a lack of high-temperature and high-pressure visualization microscopic models limits the intuitive description of flue gas-assisted steam flow characteristics. In this work, we evaluated the flow resistance and heat transfer of flue gas/flue gas + steam with a one-dimensional sandpack and explored the influence of flue gas on the flow ability of steam in porous media. A micro-experiment of flue gas-assisted steam flooding was carried out using a specially customized micro-visualization model, the flow characteristics of steam under the action of flue gas were observed and analyzed, and the key mechanism for explaining the experimental seepage phenomenon was proposed.

2. Experimental Section

2.1. Materials

The crude oil used in the experiment was taken from the Shengli oil field, with a reservoir permeability of 2000–4000 mD. Its viscosity at 50 °C was 1760 mPa·s and density was 947.8 kg/m^3 after degassing. The gas used in the experiment was flue gas, consisting of N_2 and CO_2 with 99.9% purity (Qingdao Tianyuan Gas Manufacturing Company, Qingdao, China). The volume ratio of N_2 to CO_2 was set to 4:1, with reference to the gas components emitted from the oil-field steam boiler [18]. The water used for steam production in the experiment was ultra-pure water after the ion-removal treatment of the water purifier, with a resistivity of 15 MΩ·cm. The sandpack models in the experiment were filled with 80 mesh and 120 mesh quartz sand at a 1.5:1 mass ratio; its physical parameters were basically the same, with a permeability of about 2600 mD and a porosity of about 44%, as shown in Table 1. The permeability of the sandpack refers to the ability of the model to allow fluid to pass axially under a certain pressure difference, and is a parameter that characterizes the ability of porous media to conduct liquid.

Table 1. Scheme of flow capacity evaluation experiment.

Displacement Mode	Flue Gas to Steam Ratio	Porosity/%	Permeability/10^{-3} μm^2	Steam Injection Rate (mL·min^{-1})	Flue Gas Injection Rate (mL·min^{-1})
Steam flooding	/	43.4	2661	3	0
Flue gas-assisted steam flooding	1:2	44.07	2631	3	1.5
	1:1	43.42	2558	3	3
	2:1	44	2719	3	6

2.2. Apparatus

The experimental device for the flow characteristics of flue gas-assisted steam flooding was composed of an injection system, porous media models, and a data processing and acquisition system. The injection system could inject three fluids—gas, steam, and liquid—into the porous media model. During the gas injection, the high-pressure flue gas stored in the piston container (model 1.5 L, Jiangsu Hai'an Petroleum Technology Instrument Co., Ltd., Hai'an, China; pressure range of 0.1–32 MPa; temperature range of 0~200 °C) was injected into the porous media model at a specific flow rate after passing through a gas mass flowmeter (model Sla5861, Brooks, Seattle, WA, USA; flow control range of 0–20 mL/min; accuracy of 1% of the full range). During the steam injection, deionized water was pumped by a high-precision plunger pump (Model 100DX, Teledyne Co., Ltd., Thousand Oaks, CA, USA; flow accuracy < 0.25 μL/min; pressure accuracy of ± 0.5%), which provided power and was fired by a steam generator (model GL-1, Hai-an Petroleum Equipment Company, Nantong, China; temperature range of 100–350 °C; pressure range of 0.1–25 MPa) to meet the experimental requirements, and then flowed into the porous media model. In order to ensure the quality of steam flowing into the model, the pipeline between the steam generator and the seepage model was wrapped in a heating belt with a controllable temperature. During the liquid injection, crude oil and water were, respectively, stored in the piston container and pressurized by the piston pump; they then flowed into the model. The porous medium models included a one-dimensional sandpack (see Figure 1) and a two-dimensional microscopic visualization model. The main body of the microscopic visualization model (customized, Tuochuang Scientific Research Instrument Co., Ltd., Nantong, China; temperature range of 0–280 °C; pressure range of 0.1–3 MPa) was composed of two quartz glass plates at the top and bottom. There was a hole through the glass at each of the four corners of the glass plate, which could be used as the injection end and the extraction end, as shown in Figure 2a. Porous media with different pore throat structures could be simulated by laying glass beads between the two glass plates with heat-resistant waterproof double-sided adhesive, which were then sealed with high-temperature graphite, clamped, and fixed onto two hollow metal frames, as shown in

Figure 2b,c. The length and width of the visible area of the micro-visualization model were both 25 cm and the thickness of the filled glass microspheres was less than 1 mm, which greatly increased the transparency of the model and facilitated the observation and capture of details during the flow process. The data processing and acquisition system consisted of two modules: a liquid production collection device and a real-time image collection device. The liquid production collection device was used to record the characteristics of oil and water production during the whole experiment and a temperature gun (Model DT-8867H, Huashengchang Technology Co., Ltd., Shenzhen, China; temperature range of −50–1650 °C; measuring accuracy of ± 1.0%) was used to record the temperature at the inlet and outlet of the sandpack. In the process of the microscopic visualization experiment, a high-definition digital camera was used to record the flow characteristics of the flue gas and steam. A schematic of the experimental devices is shown in Figure 3.

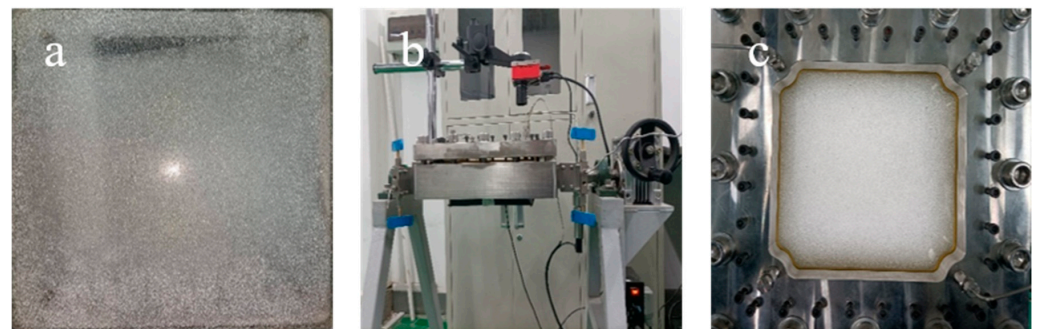**Figure 1.** One-dimensional sandpack: (**a**) lateral view, (**b**) end view.

Figure 2. Microscopic visualization model: (**a**) quartz glass plate, (**b**) lateral view, (**c**) vertical view.
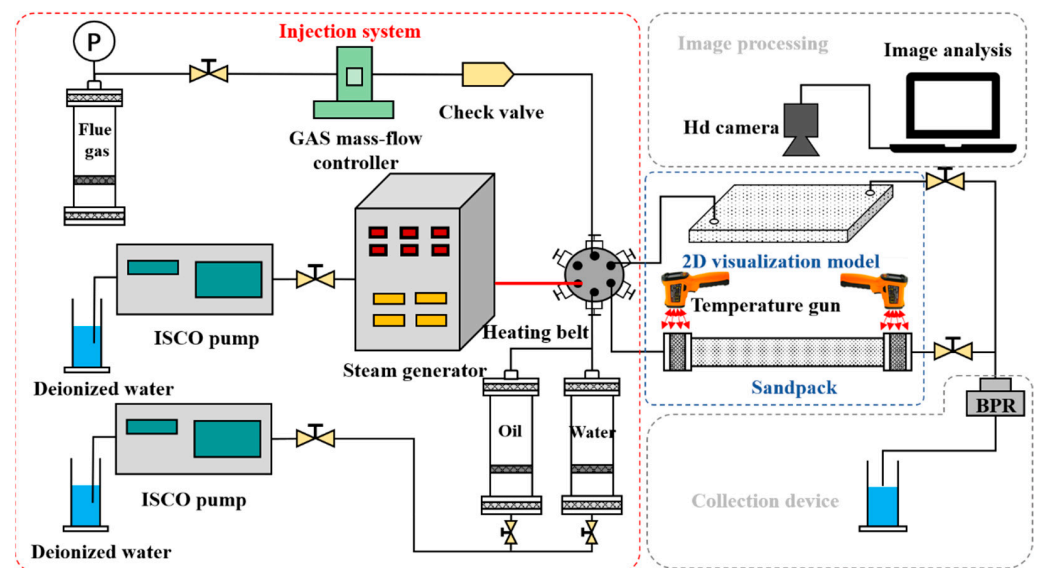

Figure 3. Schematic of experimental devices.

2.3. Experimental Procedures

2.3.1. Flow and Heat Transfer Experiments

The dissolution of flue gas in crude oil reduces the viscosity of crude oil. The CO_2 in the flue gas fraction is more soluble, especially in crude oil, which has a greater effect on the viscosity of crude oil, and the repulsion resistance will be affected to a large extent. In order to more accurately evaluate the flow ability of both repellents in porous media and to ensure a single control variable, water was used as the saturating medium for the sandpack; the experimental steps are shown below.

(1) After ensuring good air tightness, the sandpack model was prepared and the dry weight of the sandpack was measured, connected to a vacuum pump, and vacuumed. (2) We fully saturated the evacuated sandpack with water, weighed the weight of the sandpack after being saturated with water, calculated the pore volume, and measured the permeability with water. Note that the sandpack was not saturated with oil after this. (3) The steam generator was turned on and preheated in advance and the temperature was set at 150 °C. When the steam temperature and flow rate were stable, the experiment started. Steam and flue gas were injected according to the experimental design parameters and the steam injection rate was calculated by the equivalent water. (4) During the experiment, a temperature gun was used to monitor and record the inlet and outlet temperatures on the sandpack. The displacement pressure difference at both ends of the sandpack was also recorded. When the temperature in the sandpack was stable, the experiment was stopped. (5) The sand filling pipe was re-prepared and steps (1)–(4) were repeated until all the experiments in the design scheme were completed. (6) The pipelines and equipment were dismantled and cleaned, and the relevant experimental data were sorted. The experimental scheme is shown in Table 1.

2.3.2. Two-Dimensional Microscopic Visualization Experiment

(1) Double-sided adhesive was laid on the surface of the quartz glass plate and a layer of 40 mesh glass beads was pasted on it. After the two glass plates were buckled together, they were clamped and fixed onto two hollow metal frames, and the air tightness was checked after the preparation. (2) Deionized water was injected into the visualization model at a flow rate of 0.05 mL/min using an ISCO plunger pump until stable water production occurred at the outlet. The porosity was calculated from the recorded volume of saturated water. (3) After the completion of saturation of water, the dehydrated and degassed crude oil was uniformly injected into the visual model according to the experimental design parameters until the oil content of the output liquid at the outlet was 100%. The model was then aged for 24 h. (4) The steam generator was preheated in advance and the temperature was set at 150 °C. When the temperature of the steam generator was stable, the experiment started. Steam was injected into the visual model according to the experimental design parameters. (5) When the water content of the liquid produced by the steam drive reached 95%, the pure steam flooding was converted into flue gas-assisted steam flooding. The temperature of the steam remained unchanged at 150 °C and the volume ratio of the flue gas to steam was 1:1, until the water content of the liquid produced was more than 95%. (6) After the displacement process, the experimental data were sorted for the analysis. During the whole experiment, a camera was used to record in real-time. The experimental scheme is shown in Table 2.

Table 2. Scheme of microscopic visualization experiment.

Displacement Mode	Steam Temperature/°C	Porosity/%	Permeability/10^{-3} μm^2	Steam Injection Rate (mL·min^{-1})	Flue Gas Injection Rate (mL·min^{-1})
Steam flooding				0.2	0
Flue gas-assisted steam flooding	150	34.6	2450	0.2	0.2

3. Results and Discussion

3.1. Flow Capacity and Heat Transfer Effect

In order to compare the effect of flue gas on the flow capacity of steam in porous media, an analysis was carried out with the help of an evaluation of the displacement pressure difference.

The flow capacity of foam in a reservoir is generally characterized by the resistance coefficient [39,40], which can reflect the sealing effect of foam on a macroscopic scale. The resistance coefficient of foam is numerically expressed as the ratio of the pressure difference at both ends of the core to the water displacement pressure difference when the injected foam system reaches a steady state. Here, mobility was introduced to characterize the resistance of the displacement process. The mobility was expressed as the ratio of the pressure difference at both ends of the sandpack and the water flooding pressure difference under steam or flue gas-assisted steam flooding, as in Equation (1).

$$RF' = \frac{\Delta p'_f}{\Delta p_w} \tag{1}$$

where RF' is the dimensionless mobility; $\Delta p'_f$ is the pressure difference between the two ends of the sandpack during steam/flue gas-assisted steam flooding in MPa; and Δp_w is the water flooding pressure difference in MPa. The water flooding pressure difference measured in the experiments was 11 kPa.

Figure 4 shows the curve of the mobility versus the injection volume when mixing the flow of different flue gas ratios and steam. In the early and middle stages of the displacement experiment, the sandpack was in a saturated water state at the initial stage and the flow belonged to a liquid single-phase flow. The injection of steam/flue gas + steam inevitably transformed the liquid single-phase flow into a gas/vapor–liquid two-phase flow, increasing the flow resistance. Therefore, with an increase in the fluid injection volume, the mobility of the mixed fluid displacement with different flue gas ratios linearly increased. When the heat injection and dissipation in the displacement process reached a balance, a stable mainstream channel was formed and the flow resistance gradually stabilized. The mobility increased fastest in the pure steam flooding process, reaching a stable value of 9.0. As the flue gas ratio increased, the rate of increase and the stable value of the mobility gradually decreased; the mobilities were 6.2, 5.5, and 5.0 for the stable flue gas to steam volume ratios of 1:2, 1:1, and 2:1, respectively. This indicated that the addition of flue gas could reduce the flow resistance of steam.
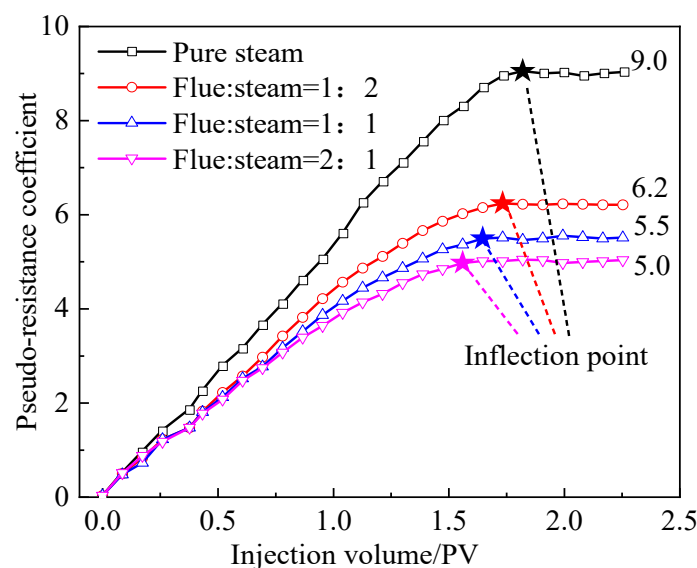

Figure 4. Mobility variation curve with steam injection volume.

We compared the mobility stability time for a mixed steam flow with different flue gas contents, as shown in Figure 5. In the pure steam displacement, when the fluid injection volume was 1.83 PV, the mobility tended to be stable. When the volume ratio of the flue gas to steam was 1:2 and the injection volume was 1.74 PV, the mobility tended to be stable and the stabilization time gradually advanced with an increase in the flue gas ratio. When the ratio of flue gas to steam was 2:1, the stabilization time was 1.56 PV. This showed that the existence of flue gas helped to accelerate the flow of steam in the reservoir and accelerate the displacement stability. This phenomenon intensified with an increase in the flue gas content.
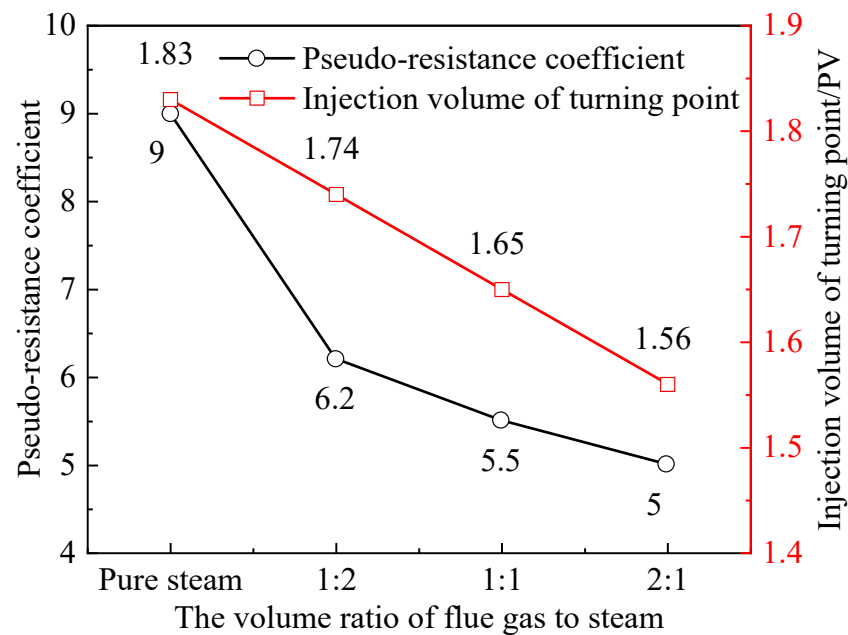

Figure 5. Comparison of stabilization time of mobility for different flue gas ratios.

The temperature field could reflect the flow state of steam in porous media. Figure 6 shows the distribution of the temperature field of flue gas-assisted steam flooding with different contents during the evaluation of flow capacity. The left side of the sandpack model was the inlet of the fluid and the right side was the outlet. At the end of the displacement, it could be seen that the temperature at the left end of the model was high; the temperature sharply dropped at the in the left third of the model position and the latter half was basically below 50 °C. With the flue gas-assisted steam flooding, the distance of heat transmission significantly increased; the position of the temperature reduction shifted to the right and changed from a sudden drop to a slow drop. When the ratio of flue gas to steam was 2:1, the temperature at the end of the model outlet was close to the inlet and the overall color was red. At the same time, according to the distribution of the temperature field, the fluid state in the core pipe after stabilization during the steam drive could be divided into three types: the steam section; the steam liquefaction section; and the saturated water section, of which the liquefaction section was the main part. With the flue gas-assisted steam flooding, under the effect of the flue gas, the gas–liquid two-phase flow at the front end of the model was converted into a gas–steam flow and the distance of the steam flow in the vapor state was lengthened. After stabilization, there were only the gas–steam section and the steam liquefaction section. This was the reason that the steam flow resistance decreased after flue gas was added, as shown in Figures 4 and 5.
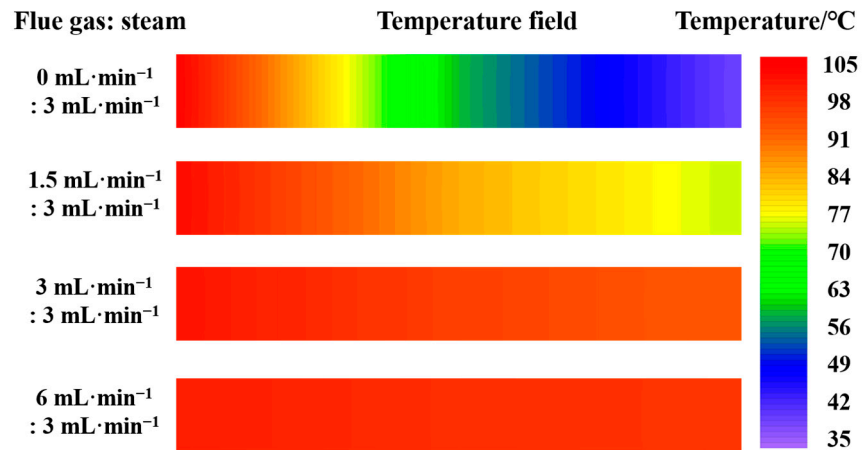
Flue gas: steam **Temperature field** **Temperature/°C**

Figure 6. Temperature field distribution (flue gas injection rate was measured at operating temperature and pressure, and steam injection rate was measured in terms of equivalent condensate).

In order to quantitatively compare the influence of flue gas on the steam heat transfer effect, the specific temperatures at the inlet and outlet of the sandpack in the four groups of displacement experiments were recorded. Combined with Figure 7, it was found that at the end of the experiment, as the proportion of flue gas increased, the temperature at the inlet of the sand-filled pipe slightly decreased from 104 °C to 100.3 °C whereas the outlet temperature significantly increased, in contrast to the pattern presented by the inlet. During the pure steam displacement, the outlet temperature was only 40 °C. With the increase in the proportion of flue gas in the injected fluid, the higher the outlet temperature was, reaching 97.3 °C, which was only 3 °C from the inlet. This phenomenon was due to the strong seepage ability of the flue gas, which was prone to a fingering phenomenon, so the steam reached the outlet faster. The existence of flue gas could inhibit steam condensation near the inlet, strengthen the heat transfer in the deep part of the reservoir, reduce steam heat loss [41], and make the heat of the steam spread to a deeper formation.
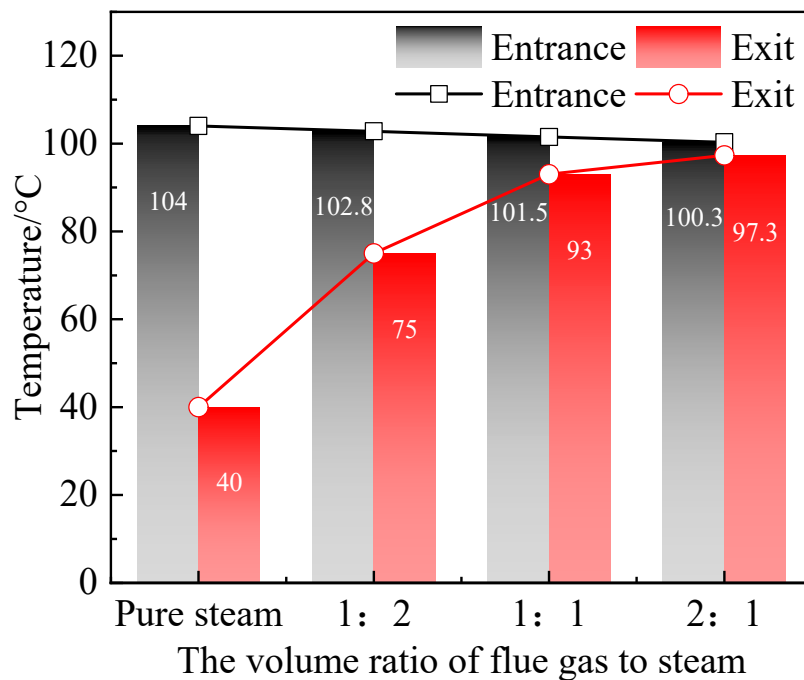

Figure 7. Variation in inlet and outlet temperatures with flue gas ratio at the end of the experiment.

3.2. Microscopic Flow Characteristics

3.2.1. Oil Displacement Dynamics and Sweep Variation

The visualized model of the saturated oil process is shown in Figure 8, with the inlet in the lower right corner and the outlet in the upper left corner of the model. As the viscosity of the injected heavy oil was much greater than the saturated water in the model, the leading edge of the heavy oil in the figure extended evenly without an obvious protrusion. The shape of the saturated oil-swept zone was regular and arc-shaped, and it smoothly advanced outward, which conformed to the theory of seepage mechanics and showed that the model had good seepage performance.
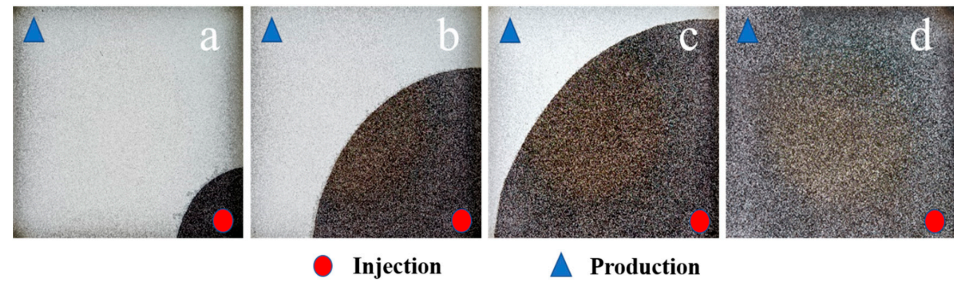

Figure 8. Saturated oil process: (**a**) 30 min, (**b**) 150 min, (**c**) 240 min, (**d**) 390 min.

Figure 9 shows the dynamic oil displacement characteristics during steam flooding and flue gas-assisted steam flooding. The black line in the figure represents the change of the displacement pressure difference with the injection volume and the red line represents the change of the recovery degree with the injection volume. It can be seen from the figure that in the steam flooding stage, with the injection of high-temperature steam, the recovery factor of heavy oil continued to increase. When the steam injection volume reached 1.1 PV, the cumulative recovery factor was 23.5% and the heavy oil recovery rate remained basically unchanged. At the same time, the displacement pressure difference in the model rapidly rose at the beginning of the steam injection because the heavy oil saturated in the model had a high viscosity and poor flow ability, which required a high displacement pressure to push the heavy oil forward. When the steam injection volume was 0.3 PV, the displacement pressure difference inside the model was 840 KPa. When the steam injection volume reached 1.2 PV, the displacement pressure difference inside the model was basically stable at 165 KPa.
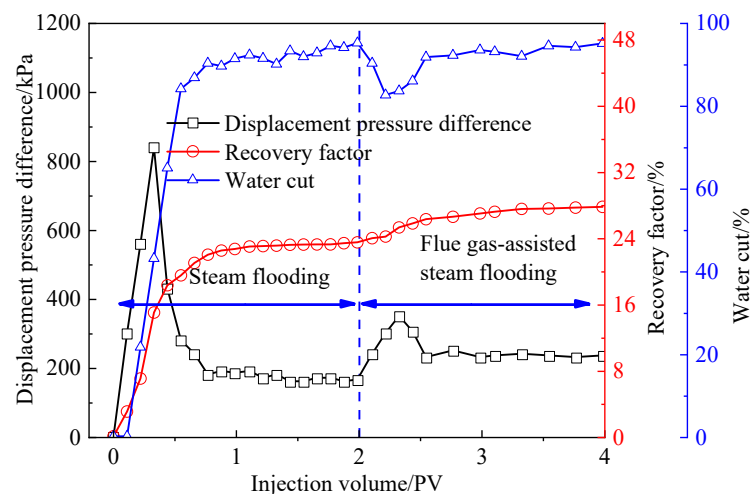

Figure 9. Variation in oil recovery and displacement pressure difference with steam-injected volume (the arrows indicate the different types of oil displacement, the dotted line represents the timing of the change of oil displacement method).

When the steam injection volume reached 2.0 PV, the water cut of the produced liquid exceeded 95%, at which point the pure steam flooding was converted into flue gas-assisted steam flooding. As can be seen from the figure, after switching the displacement mode, both the displacement pressure difference and recovery factor significantly increased. The final recovery factor finally reached 27.8%, which was 4.7% higher than that of steam flooding, and the displacement pressure difference stabilized at 230 kPa. The displacement pressure difference rapidly rose when the displacement mode was changed, reaching 350 kPa at the highest. This was because the flue gas had a strong flow capacity, opening up a new flow channel and increasing the swept area. In the swept range, the remaining oil was also further produced, greatly improving the oil displacement efficiency.

Figure 10 shows the variations in the steam wave and efficiency during steam flooding and flue gas-assisted steam flooding, where Figure 10a,b are the steam flooding process and Figure 10c is the flue gas-assisted steam flooding process. From the figure, it could be seen that due to the large difference in oil and water viscosity and the pressure between the inlet and outlet in the model, there was an obvious viscous fingering phenomenon in the model with the injection of steam and condensed hot water, and the injected fluid advanced in the direction of the main flow line toward the outlet.
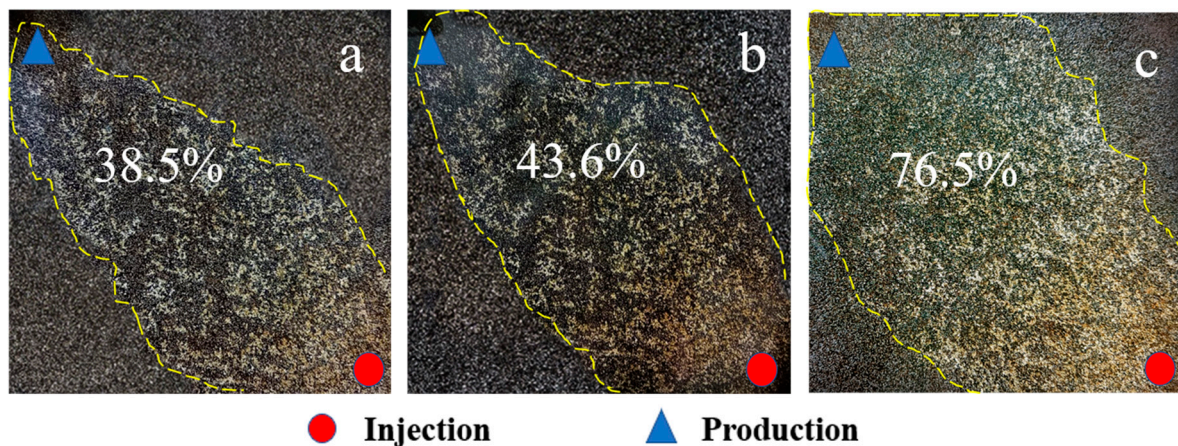

Figure 10. Plane sweep variation in steam flooding and flue gas-assisted steam flooding: (**a**) early stage of steam flooding; (**b**) end of steam flooding; (**c**) flue gas-assisted steam flooding.

From Figure 10a, it could be seen that there was a large amount of unutilized heavy oil on both sides of the main flow channel, which was caused by the channeling of steam and condensing hot water. The formation of the main flow channel had a strong inhibitory effect on the expansion of the flow channels in other directions. With the further injection of high-temperature steam and the constant equilibrium change of the pressure distribution in the model, the swept area of steam and condensing hot water changed to a certain extent, as shown in Figure 10b; the plane sweep efficiency was 43.6% at this time. The steam flooding stage of heavy oil recovery mainly relied on high-temperature steam to play the roles of heating and viscosity reduction, but due to the gradual increase in heat loss during the steam transportation process, the sweep efficiency of the steam injection alone was more limited.

When steam and flue gas were mixed, the injected fluid still displaced the heavy oil in the direction of the main flow line. With the continuous injection of steam and flue gas, the displacement area near both sides of the main flow channel changed to a certain extent, which was due to the strong percolation ability of the flue gas, making the oil sweep area significantly expand and heavy oil was further recovered, as shown in Figure 10c; the oil sweep efficiency reached 76.5%. After a further comparison, it was found that the streamline density of the extended area was much less than the original area and the quality of the flow through the steam was lower, resulting in a significant reduction in the oil-washing capacity, which explained the recovery increase of only 4.2%.

3.2.2. Flow Characteristics

Figure 11 shows the typical micro-distribution of oil and water in the thermal swept area after the completion of pure steam displacement, in which the black area is heavy oil, the white bright area is the steam displacement part, and the round spherical spots are filled glass beads. It can be seen from the figure that after the steam flooding, the remaining oil was distributed in the model in two forms: one was the corner remaining oil formed by incomplete steam or condensing hot water flooding due to the difference in oil–water viscosity [42] as shown in area A in Figure 11; the other was the blocky remaining oil formed by the steam bursting in the direction of least resistance along the course under the displacement, avoiding the area of higher resistance [43], as shown in area B in Figure 11. The former was related to the oil layer wettability and pore throat structure; the surface of the double-sided adhesive used in the experiment was lipophilic and the glass beads were randomly distributed on the double-sided adhesive during the modeling process. The latter was related to the microscopic heterogeneity of the pore structure, leading to the bypassing of the steam through the area of patches of small pore channels with high resistance.
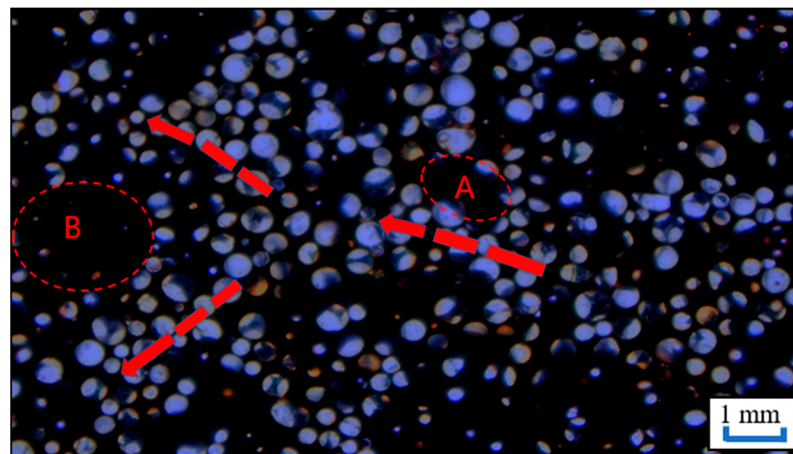

Figure 11. Micro-distribution of oil and water after steam flooding (area A represents the corner remaining oil, area B represents blocky remaining oil).

Figure 12 presents the expansion of the flow channel under the action of the flue gas, which was a typical pattern observed in the experiments. Figure 12a was taken from the position of the leading edge of the repulsion at the end of the pure steam flooding. Due to the relatively high mobility ratio of oil and water, high-permeability channel A was formed when the steam flowed and the remaining oil on both sides was blocky. After the mixed injection of flue gas and steam, the high-permeability channel was preferentially occupied and the mixed fluid was forced to open a new flow channel B whilst enhancing the oil displacement efficiency of high-permeability channel A, as shown in Figure 12b. The expansion of the fluid channels targeted the blocky remaining oil. The large area of blocky remaining oil was gradually stripped and divided, and the macroscopic effect was the expansion of the thermal swept area. The reasons for this phenomenon included two aspects: (1) the flow process gas was truncated into dispersed bubbles by the porous media in the oil–water phase, which generated the Jamin effect [44] and increased the flow resistance of the high-permeability channel; (2) the experiment was carried out under the premise of a constant heat injection, and the injection of the flue gas undoubtedly increased the total flow rate of the injected fluid and the displacement force relatively increased.
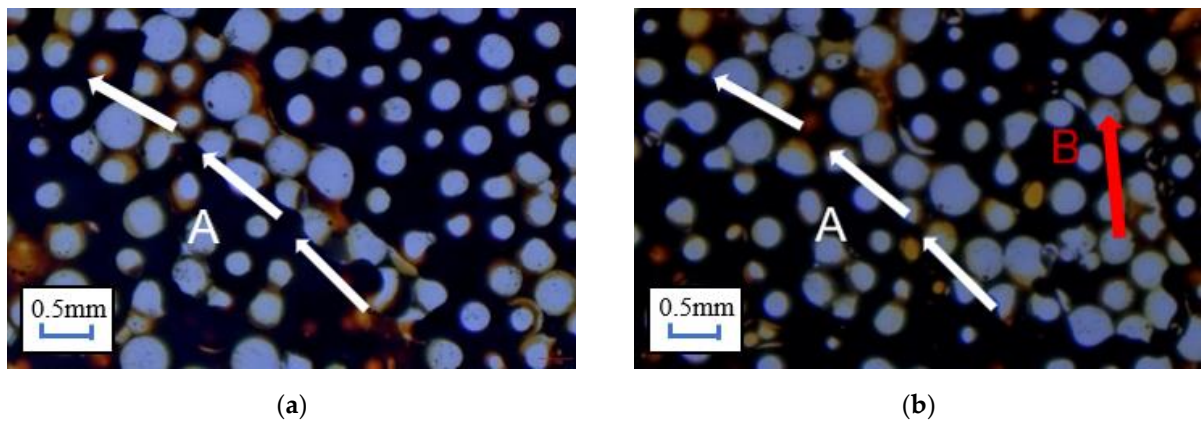
(**a**)   (**b**)

Figure 12. Expansion of flow channel under the action of flue gas: (**a**) steam flooding, (**b**) flue gas-assisted steam flooding (A is high-permeability channel, B is the newborn channel under the action of flue gas).

It is worth noting that when flue gas and steam are mixed and injected, flue gas will exist in the oil–water phase in the form of bubbles. As shown in Figure 13, the flow of bubbles scratched and extracted the remaining oil in the pores. In addition, the contact efficiency between the flue gas and heavy oil was higher. The dissolution and release process in heavy oil can destroy the molecular network structure of heavy oil to a certain extent, reduce the viscosity of heavy oil, and improve the flow ability of heavy oil. In summary, the mobilization mechanism of the corner remaining oil and blocky remaining oil after steam flooding resulted in: (1) the expansion of the fluid channel; (2) the flow of gas bubbles in the flue; and (3) the flue gas being dissolved and released in heavy oil.
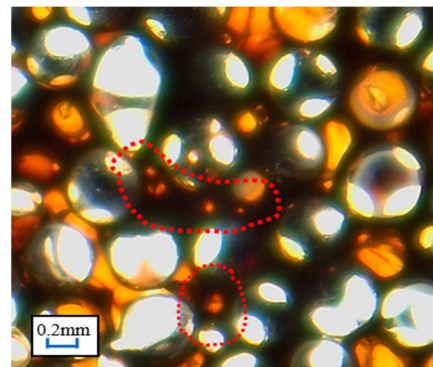

Figure 13. Bubble flow in remaining oil (the red dotted line marks flue gas bubbles in heavy oil).

4. Conclusions

Flue gas has a significant effect on the flow of steam in porous media. This work analyzed the reasons for the increased steam heat transfer efficiency of flue gas from a flow perspective and discussed the flow variability characteristics that led to an improved sweep efficiency and recovery from a microscopic perspective. The following conclusions were drawn.

1. The flue gas could reduce the flow resistance of steam whilst accelerating its flow. Compared with pure steam, the flow rate of flue gas to steam with a volume ratio of 1:2 was reduced by 2.8 and the stabilization time was advanced by 0.09 PV. This phenomenon intensified as the proportion of flue gas increased.
2. The fingering effect of the flue gas could promote the steam flow, make the steam reach the deep part of the sandpack faster, reduce the heat loss along the way, and thus transfer more heat to the deep part of the model. When the volume ratio of flue

gas to steam was 2:1, the temperature at the outlet of the model increased by 57.3 °C compared with pure steam.

3. Due to the expansion of fluid channels, the flow of flue gas foam, and the effective utilization of blocky remaining oil and corner remaining oil during the dissolution and release of flue gas in heavy oil, the recovery and sweep efficiency of the flue gas and steam mixed injection increased by 4.7% and 32.9%, respectively, compared with the pure steam injection stage.

The findings of this work will help to improve the comprehensive interpretation of field test data, leading to more adapted construction schemes. However, the proportion of flue gas added to the steam in this work was relatively small, and a larger proportion of flue gas mixed injection tests needs to be carried out. The priority of the two mechanisms (flue gas inhibiting steam condensation and improving the steam flow capacity) of flue gas for improving steam heat transfer has yet to be clarified.

Author Contributions: Conceptualization, Y.J. and B.L. (Boliang Li); methodology, Y.J. and B.L. (Binfei Li); software, B.L. (Boliang Li); validation, B.L. (Binfei Li) and B.L. (Boliang Li); formal analysis, Y.J.; investigation, Y.J. and B.L. (Boliang Li); resources, Z.H., J.W. and B.L. (Binfei Li); data curation, Y.J. and B.L. (Boliang Li); writing—original draft preparation, Y.J.; writing—review and editing, B.L. (Boliang Li); visualization, B.L. (Binfei Li); supervision, B.L. (Binfei Li); project administration, B.L. (Binfei Li) and Z.L.; funding acquisition, B.L. (Binfei Li) and Z.L. All authors have read and agreed to the published version of the manuscript.

Data Availability Statement: All data used to support the findings of this study are included within the article.

Conflicts of Interest: The authors declare that they have no known competing financial interest or personal relationships that could have appeared to influence the work reported in this paper.

References

1. Briggs, P.; Baron, P.; Fulleylove, R.; Wright, M. Development of heavy-oil reservoirs. *J. Pet. Sci. Eng.* **1988**, *40*, 206–214. [CrossRef]
2. Santos, R.; Loh, W.; Bannwart, A.; Trevisan, O. An overview of heavy oil properties and its recovery and transportation methods. *Braz. J. Chem. Eng.* **2014**, *31*, 571–590. [CrossRef]
3. Langevin, D.; Poteau, S.; Hénaut, I.; Argillier, J. Crude oil emulsion properties and their application to heavy oil transportation. *Oil Gas Sci. Technol.* **2004**, *59*, 511–521. [CrossRef]
4. Wilson, R.; Mercier, P.H.; Patarachao, B.; Navarra, A. Partial least squares regression of oil sands processing variables within discrete event simulation digital twin. *Minerals* **2021**, *11*, 689. [CrossRef]
5. Liu, Z.; Wang, H.; Blackbourn, G.; Ma, F.; He, Z.; Wen, Z.; Wang, Z.; Yang, Z.; Luan, T.; Wu, Z. Heavy oils and oil sands: Global distribution and resource assessment. *Acta Geol. Sin.* **2019**, *93*, 199–212. [CrossRef]
6. Zyrin, V.; Ilinova, A. Ecology safety technologies of unconventional oil reserves recovery for sustainable oil and gas industry development. *J. Ecol. Eng.* **2016**, *17*, 35–40. [CrossRef]
7. Altunina, L.; Kuvshinov, V.; Stasyeva, L.; Kuvshinov, I. Trends and prospects of physicochemical methods for enhanced oil recovery of heavy oil fields. *Chem. Sustain. Dev.* **2018**, *26*, 240–255. [CrossRef]
8. Zhao, D.; Wang, J.; Gates, I.D. Thermal recovery strategies for thin heavy oil reservoirs. *Fuel* **2014**, *117*, 431–441. [CrossRef]
9. Nasr, T.N.; Ayodele, O.R. Thermal Techniques for the Recovery of Heavy Oil and Bitumen. In Proceedings of the SPE International Improved Oil Recovery Conference in Asia Pacific, Kuala Lumpur, Malaysia, 5–6 December 2005. SPE-97488-MS.
10. Guo, K.; Li, H.; Yu, Z. In-situ heavy and extra-heavy oil recovery: A review. *Fuel* **2016**, *185*, 886–902. [CrossRef]
11. Xu, A.; Meng, L.; Fan, Z.; Zhao, L. New findings on heatloss of superheated steam transmitted along the wellbore and heating enhancement in heavy oil reservoirs. In Proceedings of the International Petroleum Technology Conference, Beijing, China, 26–28 March 2013; IPTC-16439-MS.
12. Cao, Y.; Liu, D.; Zhang, Z.; Wang, S.; Wang, Q.; Xia, D. Steam channeling control in the steam flooding of super heavy oil reservoirs, Shengli Oilfield. *Petrol. Explor. Dev.* **2012**, *39*, 785–790. [CrossRef]
13. Hunter, B.; Buell, R.; Abate, T. Application of a polymer gel system to control steam breakthrough and channeling. In Proceedings of the SPE Western Regional Meeting, Bakersfield, CA, USA, 30 March–1 April 1992; SPE-24031-MS.
14. Shah, A.; Fishwick, R.; Wood, J.; Leeke, G.; Rigby, S.; Greaves, M. A review of novel techniques for heavy oil and bitumen extraction and upgrading. *Energ Environ. Sci.* **2010**, *3*, 700–714. [CrossRef]

15. Canbolat, S.; Akin, S.; Kovscek, A. Noncondensable gas steam-assisted gravity drainage. *J. Petrol. Sci. Eng.* **2004**, *45*, 83–96. [CrossRef]
16. Huang, Y.; Xiao, W.; Chen, S.; Li, B.; Du, L.; Li, B. A Study on the Adaptability of Nonhydrocarbon Gas-Assisted Steam Flooding to the Development of Heavy Oil Reservoirs. *Energies* **2022**, *15*, 4805. [CrossRef]
17. Fan, J.; Yang, J.; Fan, X.; Wu, L. Experimental study on the mechanism of enhanced oil recovery by non-condensable gas-assisted steam flooding process in extra-heavy oil reservoir. *Energy Sources Part A* **2021**, *43*, 444–460. [CrossRef]
18. Monte-Mor, L.; Laboissiere, P.; Trevisan, O. Laboratory study on steam and flue gas co-injection for heavy oil recovery. In Proceedings of the SPE Heavy Oil Conference-Canada, Calgary, AB, Canada, 11–13 June 2013; SPE-165523-MS.
19. Srivastava, R.; Huang, S.; Dong, M. Comparative effectiveness of CO_2, produced gas, and flue gas for enhanced heavy-oil recovery. *SPE Reserv. Eval. Eng.* **1999**, *2*, 238–247. [CrossRef]
20. Nasr, T.; Prowse, D.; Frauenfeld, T. The Use of Flue Gas with Steam in Bitumen Recovery from Oil Sands. *J. Can. Pet. Technol.* **1987**, *26*, 5–9. [CrossRef]
21. Wang, Z.; Li, Z.; Lu, T.; Yuan, Q.; Yang, J.; Wang, H.; Wang, S. Research on enhancing heavy oil recovery mechanism of flue gas assisted steam flooding. In Proceedings of the Carbon Management Technology Conference, Houston, TX, USA, 17–20 July 2017. CMTC-486093-MS.
22. Lu, T.; Ban, X.; Li, Z.; Gao, Y.; Guo, E.; Yang, J.; Ma, H.; Wang, H.; Wei, Y. Mechanisms on expansion of SAGD steam chamber assisted by flue gas. *Acta Pet. Sin.* **2021**, *42*, 1072–1080.
23. Li, H.; Yang, D.; Tontiwachwuthikul, P. Experimental and theoretical determination of equilibrium interfacial tension for the solvent (s)–CO_2–heavy oil systems. *Energy Fuels* **2012**, *26*, 1776–1786. [CrossRef]
24. Hemmati-Sarapardeh, A.; Ayatollahi, S.; Ghazanfari, M.-H.; Masihi, M. Experimental determination of interfacial tension and miscibility of the CO_2–crude oil system; temperature, pressure, and composition effects. *J. Chem. Eng. Data* **2014**, *59*, 61–69. [CrossRef]
25. Gajbhiye, R. Effect of CO_2/N_2 mixture composition on interfacial tension of crude oil. *ACS Omega* **2020**, *5*, 27944–27952. [CrossRef]
26. Chung, F.T.; Jones, R.A.; Nguyen, H.T. Measurements and correlations of the physical properties of CO_2-heavy crude oil mixtures. *SPE Reserv. Eng.* **1988**, *3*, 822–828. [CrossRef]
27. Li, S.; Li, B.; Zhang, Q.; Li, Z.; Yang, D. Effect of CO_2 on heavy oil recovery and physical properties in huff-n-puff processes under reservoir conditions. *J. Energy Resour. Technol.* **2018**, *140*, 072907. [CrossRef]
28. Jia, B.; Xian, C.; Tsau, J.; Zuo, X.; Jia, W. Status and Outlook of Oil Field Chemistry-Assisted Analysis during the Energy Transition Period. *Energy Fuels* **2022**, *36*, 12917–12945. [CrossRef]
29. Gao, Y.; Liu, S.; Shen, D.; Guo, E.; Bao, Y. Improving oil recovery by adding N_2 in SAGD process for super-heavy crude reservoir with top-water. In Proceedings of the SPE Russian Oil and Gas Technical Conference and Exhibition, Moscow, Russia, 28–30 October 2008; SPE-114590-MS.
30. Cuiyu, M.; Yuetian, L.; Peiqing, L.; Chunhong, W.; Jingli, L. Study on steam huff and puff injection parameters of herringbone well in shallow and thin heavy oil reservoir. *Open Pet. Eng. J.* **2013**, *6*, 69–75.
31. Tao, L.; Li, G.; Li, L.; Shan, J. Research and application of horizontal well infill SAGD development technology for super heavy oil reservoirs. In Proceedings of the SPE Improved Oil Recovery Conference, Virtual. 31 August–4 September 2020. SPE-200389-MS.
32. Li, Z.; Lin, R. Flow features and heat exchange laws of steam-nitrogen mixture in thermal recovery wellbore. *Acta Pet. Sin.* **2010**, *31*, 506–510.
33. Yu, J.; Li, Y. Progress in gas-water two-phase seepage and its application in water flooding gas reservoirs. *J. Southwest Pet. Univ. Sci. Technol. Ed.* **2003**, *25*, 36–39.
34. Li, Y.; Zhao, D.; Du, D. Computational study on the three phase displacement characteristics of foam fluids in porous media. *J. Pet. Sci. Eng.* **2022**, *215*, 110732. [CrossRef]
35. Lin, Y.; Yang, Q.; Liu, X. Three-phase seepage characteristics of oil, gas and water in low permeability reservoirs. *Acta Pet. Sin.* **2006**, *27*, 124–128.
36. Blunt, M.; Zhou, D.; Fenwick, D. Three-phase flow and gravity drainage in porous media. *Transp. Porous Media* **1995**, *20*, 77–103. [CrossRef]
37. Zhu, S.; Li, Y.; Zhang, R.; Tang, Y.; Qiu, L.; Zhi, X. Experimental study on the condensation characteristics of nitrogen with non-condensable gas. *Cryogenics* **2019**, *98*, 29–38. [CrossRef]
38. Wang, Y.; Wu, X.; Wang, R.; Lai, F. Study on multiple thermal fluid applied in heavy oil development. *Metal. Int.* **2013**, *18*, 98–103.
39. Wang, Y.; Liu, K.; Zhang, B.; Ling, Q. Effect of permeability on foam mobility and flow resistance distribution: An experimental study. *Colloids Surf. A* **2019**, *582*, 123769. [CrossRef]
40. Wang, X.; Chen, J.; Lv, C.; Wei, M. Experimental investigation and evaluation on influence of foam flow resistance in porous media. *Environ. Earth Sci.* **2015**, *74*, 5729–5738. [CrossRef]
41. Yi, Q.; Tian, M.; Yan, W.; Qu, X.; Chen, X. Visualization study of the influence of non-condensable gas on steam condensation heat transfer. *Appl. Therm. Eng.* **2016**, *106*, 13–21. [CrossRef]
42. Zhang, Y.; Zhao, P.; Cai, M.; Lu, F.; Wu, X.; Guo, Z. Occurrence state and forming mechanism of microscopic remaining oil controlled by dynamic and static factors. *J. Pet. Sci. Eng.* **2020**, *193*, 107330. [CrossRef]

43. Sun, H.; Zhao, Y.; Yao, J. Micro-distribution and mechanical characteristics analysis of remaining oil. *Petroleum* **2017**, *3*, 483–488. [CrossRef]

44. Wright, R. Jamin effect in oil production. *AAPG Bull.* **1933**, *17*, 1521–1526.